

Bias-stress stability and radiation response of solution-processed AlO_x dielectrics investigated by on-site measurements

Y. X. Fang^{1,2}, C. Zhao^{1,2,*}, I. Z. Mitrovic², S. Hall², L. Yang^{3,4}, C. Z. Zhao^{1,2,*}

¹Department of Electrical and Electronic Engineering, Xi'an Jiaotong-Liverpool University, Suzhou, China.

²Department of Electrical Engineering and Electronics, University of Liverpool, Liverpool, UK.

³Department of Chemistry, Xi'an Jiaotong-Liverpool University, Suzhou 215123, China.

⁴Department of Chemistry, University of Liverpool, Liverpool L69 7ZD, UK.

*E-mail address of corresponding authors: Chun.Zhao@xjtlu.edu.cn; Cezhou.Zhao@xjtlu.edu.cn

10 Abstract

11 In this work, the effects of biased
12 irradiation on solution-processed and atomic
13 layer deposited (ALD) AlO_x thin films MOS
14 capacitors were investigated by an on-site
15 technique. The devices were irradiated by a
16 662-KeV Cs^{137} γ -ray radiation source under
17 different positive/negative gate biases. The
18 radiation time was up to 10^5 s and the total dose
19 was around 92 Gy. It has been found that
20 radiation could result in reversibility of flat-
21 band voltage shifts (ΔV_{FB}) of solution-
22 processed AlO_x MOS capacitors, which were
23 further analyzed through calculating the
24 radiation induced oxide traps (ΔN_{ot}) in AlO_x
25 thin film and interface traps at AlO_x/Si
26 interface (ΔN_{it}). Additionally, solution-
27 processed AlO_x MOS capacitors exhibit more
28 radiation induced charges compared to those
29 fabricated by ALD, which indicates that
30 solution-processed AlO_x thin films contain
31 abundant precursor impurities and bonded
32 oxygen.

33 **Keywords:** Solution-processed; High- k gate
34 dielectric; AlO_x ; Biased γ -ray radiation stress
35 stability.

36 1. Introduction

37 To date, solution processes have been
38 developed due to the possibility of low-cost and
39 large-area fabrication without using vacuum
40 deposition techniques. Furthermore, solution-
41 processed high- k oxide dielectrics enable low
42 leakage current, low operation voltage and ease
43 of process integration for associated thin-film
44 transistors (TFTs) [1]. Among the various high- k
45 materials, Al_2O_3 is a promising candidate, due to
46 its good chemical stability and low
47 oxide/semiconductor interface trap density in a
48 TFT device [2]. High temperature (>300 °C)
49 annealed high- k oxide materials exhibit
50 satisfactory film quality, electrical properties and
51 reliability. However, their potential applications
52 towards wearable electronics and bioelectronics
53 are further restrained due to the high annealing

54 temperature required in the fabrication [3]. As a
55 result, it is necessary to investigate the bias-stress
56 stability and radiation response of solution-
57 processed high- k oxide materials annealed at low
58 temperature (<150 °C). In addition, low
59 temperature processing with simplified process
60 steps is the primary advantage of solution-process
61 compared to traditional vacuum fabrication
62 methods.

63 In general, for a TFT, ionizing radiation could
64 lead to device degradation by generating bulk
65 oxide and interface traps near the
66 oxide/semiconductor interface [4]. There have
67 been few reported studies addressing radiation
68 damage to solution-processed high- k materials
69 for TFT application [5]. It should be noted that the
70 interruption of irradiation in conventional off-site
71 radiation response measurements can cause a
72 rapid recovery of flat band voltage (V_{FB}) shift so
73 that the degradation caused by charge
74 trapping/de-trapping of the devices is
75 underestimated [6]. As a result, on-site
76 measurements are required and to our knowledge,
77 no research has been reported on the study of γ -
78 ray radiation response of solution-processed
79 high- k materials investigated by an on-site
80 technique.

81 In this work, solution-processed and atomic
82 layer deposited (ALD) AlO_x thin films were
83 fabricated for comparison. They were integrated
84 into capacitors to investigate bias-stress stability
85 along with radiation response through the on-site
86 technique [7].

87 2. Experimental

88 2.1 Precursor Preparation

89 The precursor solution was prepared by
90 dissolving 2.5M concentration aluminum nitrate
91 hydrate ($\text{Al}(\text{NO}_3)_3 \cdot x\text{H}_2\text{O}$) in water. The solution
92 was stirred in ultrasonic bath for 2 h to ensure the
93 precursor was fully dissolved since the nitrate
94 salts show excellent water solubility. Before spin
95 coating, the solution was filtered by a 0.45 μm
96 polyether sulfone (PES) syringe filter.

97 2.2 Device fabrication

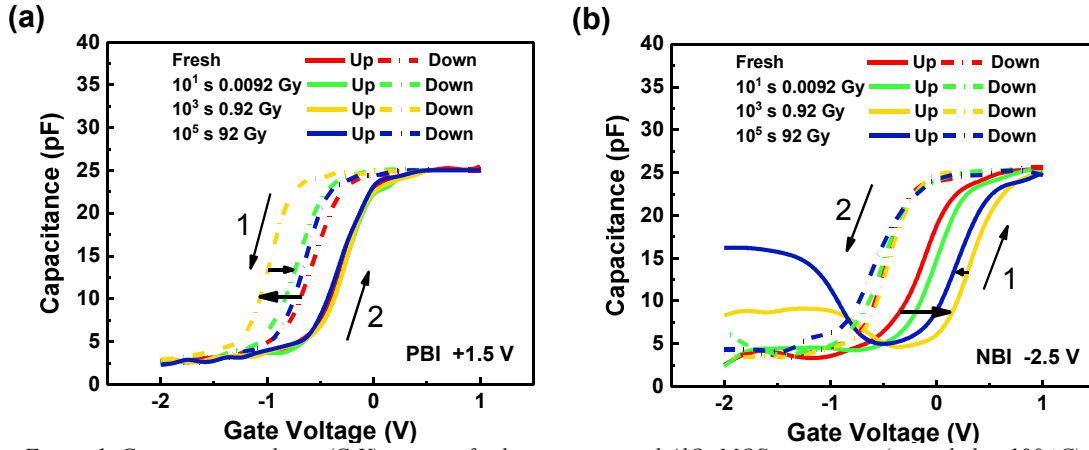


Figure 1. Capacitance-voltage (C - V) curves of solution-processed AlO_x MOS capacitors (annealed at 100°C) under 10^5 s gate bias-stress voltage of (a) $+1.5$ V positively biased irradiation (PBI) and (b) -2.5 V negatively biased irradiation (NBI). The total dose is around 92 Gy.

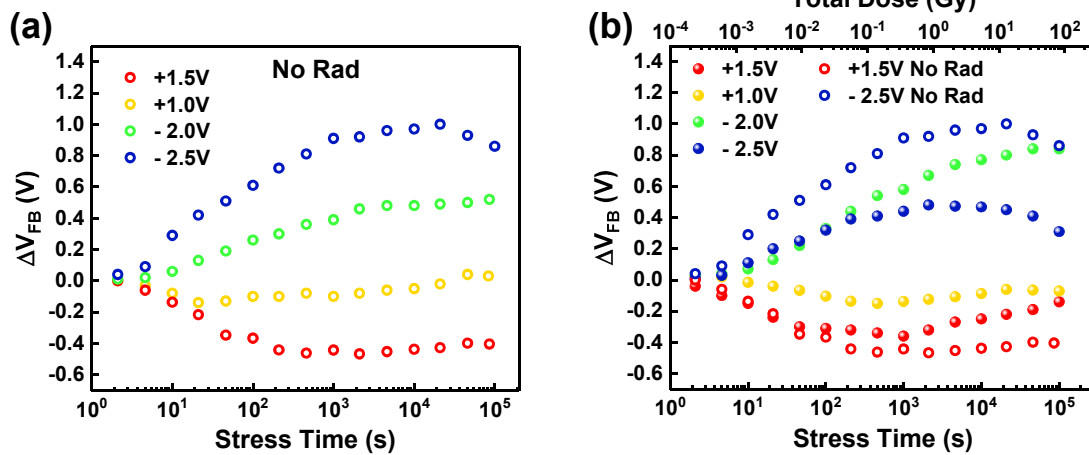


Figure 2. Flat-band voltage shift (ΔV_{FB}) of solution-processed AlO_x capacitors induced by different positive/negative bias-stress as a function of (a) stress time, (b) stress time & total dose. ΔV_{FB} was extracted from C - V curves measured from AlO_x capacitors at 1 MHz.

1
 2 Before spinning-coating, lightly-doped N type
 3 Si substrates (resistivity: $2\text{-}4 \Omega\cdot\text{cm}$, impurity
 4 density: $1.65\times 10^{15} \text{ cm}^{-3}$) were dipped in 2% HF
 5 aqueous solution for 60 s to remove the native
 6 oxide, and dried by N_2 . Subsequently, the
 7 substrates were exposed to air plasma for 15 mins.
 8 After preparation of Si substrates, the precursor
 9 solution was spin-coated on the processed
 10 substrate at 4500 rpm for 40 s. Samples were then
 11 immediately annealed on the hot plate at 100°C
 12 for 1 h in air atmosphere. Finally, 300 nm thick
 13 Al top and bottom electrodes were deposited
 14 through shadow masks by e-beam evaporation.
 15 The circular top electrode had a diameter of 0.3
 16 mm.

17 2.3 Characterization

18 The thickness of the AlO_x thin films was
 19 measured by spectroscopic ellipsometry.
 20 Solution-processed and ALD AlO_x thin films are
 21 50 nm and 40 nm thick, respectively. The
 22 capacitance-voltage (C - V) characteristics were
 23 measured using a HP 4284 precision LCR meter
 24 at a frequency of 1 MHz. To investigate the bias-

25 stress and biased irradiation stability of AlO_x
 26 MOS capacitor, constant voltage bias stress was
 27 applied on the gate with and without radiation
 28 exposure. The bias-stress voltage is the voltage
 29 applied on the gate during the bias-stress. C - V
 30 curves were measured at regular points in time of
 31 $10^{1/3}$ s, $10^{2/3}$ s, $10^{3/3}$ s, $10^{4/3}$ s, $10^{5/3}$ s etc. to allow
 32 extraction of the V_{FB} during the bias-stress. For
 33 biased irradiation, a 662-keV Cs^{137} γ -ray radiation
 34 source was used, the stress time was up to 10^5 s
 35 and the total dose was around 92 Gy. All
 36 electrical measurements were carried out in the
 37 dark at room temperature.

38 3. Results and Discussion

39 The C - V curves of solution-processed AlO_x
 40 MOS capacitors under 10^5 s gate bias-stress
 41 voltage of irradiated $+1.5$ V and irradiated -2.5 V
 42 are shown in Figs. 1 (a) and (b), respectively. It
 43 can be seen that the shift of the C - V curves,
 44 positive or negative, is determined by the gate
 45 bias stress polarity. Positively biased irradiation
 46 (PBI) and negatively biased irradiation (NBI)

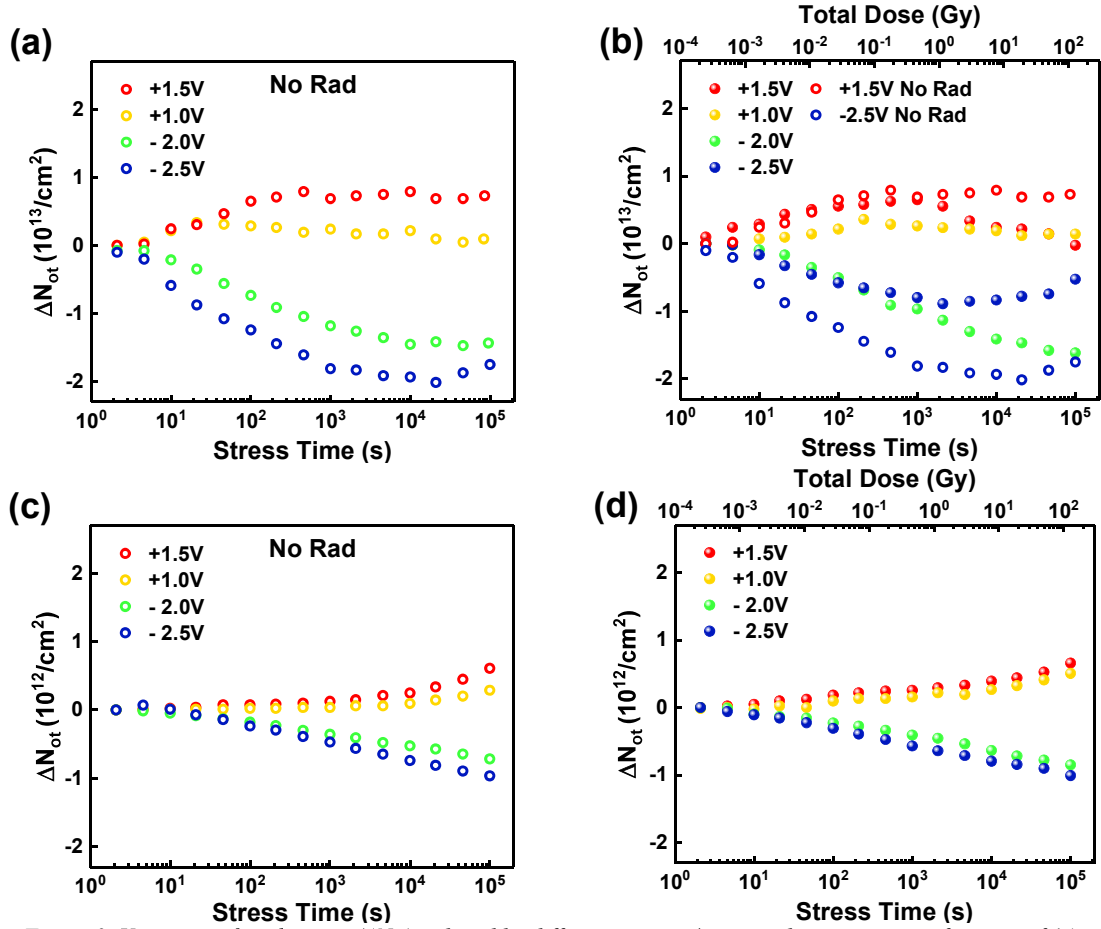


Figure 3. Variation of oxide traps (ΔN_{ot}) induced by different positive/negative bias-stress as a function of (a) stress time (solution-processed AlO_x), (b) stress time & total dose (solution-processed AlO_x), (c) stress time (ALD AlO_x) and (d) stress time & total dose (ALD AlO_x).

1

2 produce negative and positive flat-band voltage
3 shift (ΔV_{FB}), respectively. To determine V_{FB} , flat
4 band capacitance (C_{FB}) is calculated first, then left
5 flat-band voltage ($V_{FB L}$) and right flat-band
6 voltage ($V_{FB R}$) can be determined from the left
7 and right C-V curves of the MOS devices,
8 respectively. It is found in Fig. 1(a) that the
9 degradation of C-V curves is mainly caused by
10 $\Delta V_{FB L}$ under PBI. Under NBI, as shown in Fig.
11 1(b), $\Delta V_{FB R}$ dominates the device degradation.
12 Consequently, $\Delta V_{FB L}$ under PBI and $\Delta V_{FB R}$ under
13 NBI are further investigated by consideration of
14 the hysteresis. In addition, ΔV_{FB} is found to
15 increase first when the stress time is less than 10^3
16 and then decrease as the stress time increases
17 from 10^3 s to 10^5 s. This reversible behavior
18 indicates that the ΔV_{FB} is mainly caused by the
19 bias-stress induced charges in short stress time ($<$
20 10^3 s). As the stress time increases (10^3 s \sim 10^5 s),
21 the radiation generated charges becomes
22 dominant and can compensate the bias-stress
23 induced charges, thus cause ΔV_{FB} to decrease.
24 Plots of ΔV_{FB} under gate bias-stress with and
25 without radiation are shown in Fig. 2. The
26 radiation-induced ΔV_{FB} is determined by the
27 generation of oxide traps (ΔN_{ot}) in the AlO_x film

28 and interface traps (ΔN_{it}) at the AlO_x/Si interface.
29 The ΔN_{ot} causes a parallel shift of both mid-gap
30 and flat band voltages, ΔN_{it} determines the
31 stretch-out of the C-V curve and only shifts the
32 flat band voltage [8].

33 Figs. 3 (a) and (b) summarize the ΔN_{ot} of
34 solution-processed AlO_x capacitors under gate
35 bias with and without radiation. ΔN_{ot} is estimated
36 as [9]:

$$\Delta N_{ot} = -\frac{C_{ox}\Delta V_{mg}}{qA} \quad (1)$$

37 where C_{ox} is oxide capacitance, ΔV_{mg} is shift of
38 mid gap voltage, q is elemental charge and A is
39 the area of the device. Under PBI, positive ΔN_{ot}
40 decreases with increasing radiation dose,
41 indicating that the radiation has generated
42 negative oxide trapped charges. Under NBI, a
43 decrease of ΔN_{ot} can also be observed.
44 Furthermore, with a larger gate bias, the
45 decreasing of ΔN_{ot} becomes more obvious. These
46 results suggest that bias-stress enhances the effect
47 of radiation, which will be discussed later with the
48 aid of the energy band diagrams in Fig. 5. The
49 ΔN_{ot} of ALD AlO_x capacitors with and without
50 radiation are shown in Figs. 3 (c) and (d). These

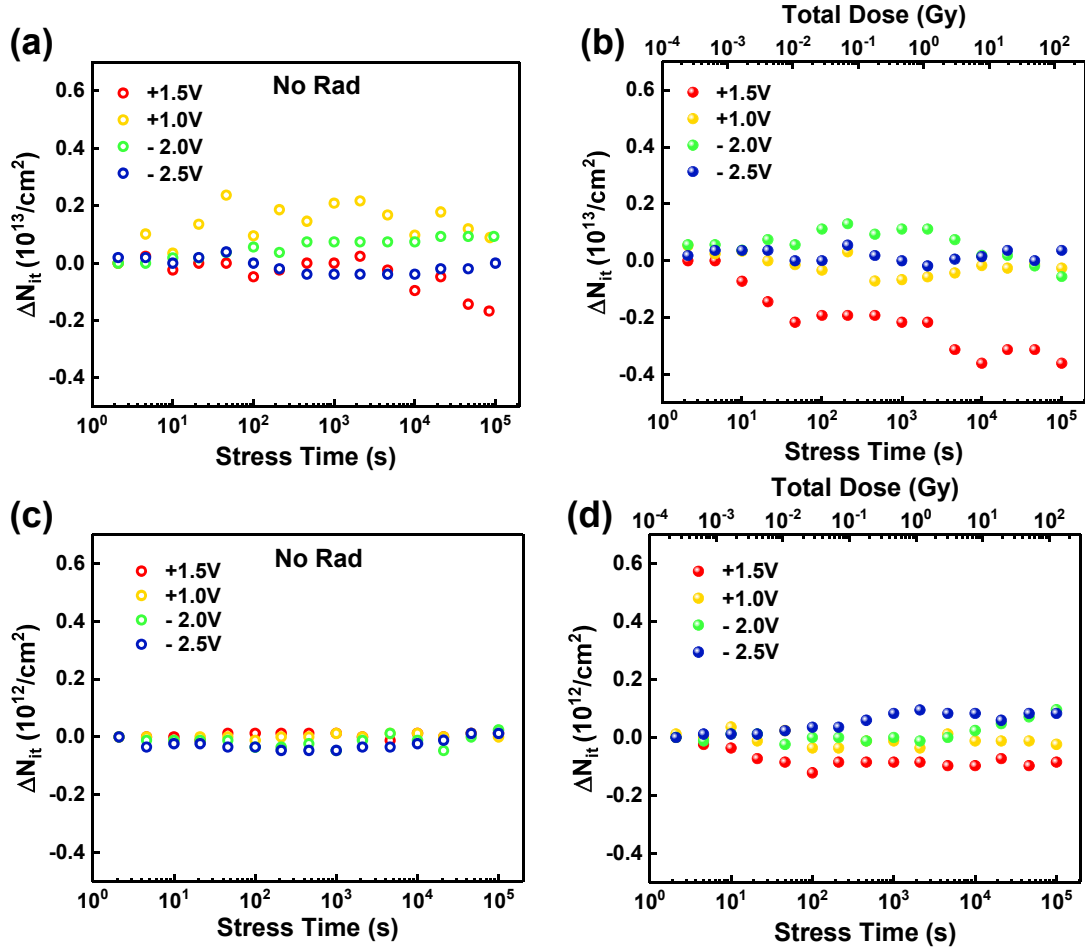


Figure 4. Variation of interface traps (ΔN_{it}) induced by different positive/negative bias-stress as a function of (a) stress time (solution-processed AlO_x), (b) stress time & total dose (solution-processed AlO_x), (c) stress time (ALD AlO_x) and (d) stress time & total dose (ALD AlO_x).

1
 2 devices reveal small ΔN_{ot} and no significant
 3 changes or reversibility are observed, indicating
 4 better radiation hardness relative to solution-
 5 process AlO_x . It is reported that solution-
 6 processed, low temperature AlO_x contains a large
 7 concentration of bonded oxygen, which could
 8 provide defect states in the bandgap of AlO_x [2].
 9 Figs. 4 (a) and (b) present the ΔN_{it} of solution-
 10 processed AlO_x capacitors under gate bias-stress
 11 with and without radiation. ΔN_{it} is estimated as
 12 [9]:

$$\Delta N_{it} = \frac{C_{ox}(\Delta V_{FB} - \Delta V_{mg})}{qA} \quad (2)$$

13 Under PBI, the devices exhibit a build-up of Si
 14 dangling bonds, which is related to the protons
 15 released by radiation. Under NBI, there is a
 16 negligible change of ΔN_{it} because PB is necessary
 17 to generate interface traps under radiation
 18 exposure. The mechanism will be explained in the
 19 next section. Furthermore, ΔN_{it} of ALD AlO_x
 20 capacitors is shown in Figs. 4 (c) and (d). Similar
 21 to the associated ΔN_{ot} results, biased irradiation
 22 generates very few interface traps. This is likely
 23 to be due to the low defect state density in ALD
 24 AlO_x thin films.

25 As ALD AlO_x thin films have exhibited
 26 satisfied radiation hardness. The radiation
 27 mechanism of solution-processed AlO_x thin films
 28 is further investigated in this work. Figs. 2 have
 29 illustrated a reversible behavior of ΔV_{FB} of
 30 solution-processed devices. The reversibility of
 31 ΔV_{FB} is associated with the combined effect of
 32 ΔN_{ot} and ΔN_{it} .

33 Fig. 5 (a) and (b) demonstrates the energy band
 34 diagrams of solution-processed AlO_x MOS
 35 capacitors under (a) PBI and (b) NBI,
 36 respectively. Under PBI, when the PBI time is
 37 shorter than 10^3 s, electrical bias causes a negative
 38 ΔV_{FB} by generating positive ΔN_{ot} and radiation
 39 exposure can barely affect the device degradation.
 40 However, as shown in Fig. 5 (a), neutral oxide
 41 traps are created in the bulk of the AlO_x during
 42 exposure to ionizing irradiation [10]. With a
 43 positively applied gate voltage, electrons in the
 44 accumulation region at the AlO_x/Si interface can
 45 tunnel into those radiation induced neutral oxide
 46 traps (process (2) in Fig. 5(a)). The effects of bias-
 47 stress and irradiation add up and form negatively
 48 charged traps, which can compensate the positive
 49 oxide trapped charges near the AlO_x/Si interface,
 50 thus reduce positive ΔN_{ot} [11, 12]. Consequently,

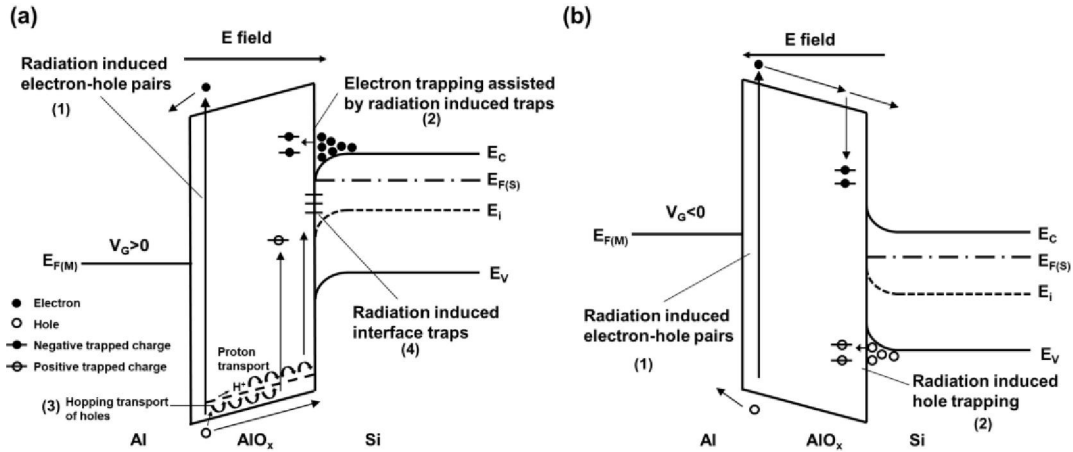


Figure 5. Energy band diagrams of solution-processed AlO_x capacitors under (a) PBI and (b) NBI.

1
 2 when the PBI time increases from 10^3 s to 10^5 s,
 3 radiation induced electron trapping among the
 4 oxide dominates the device degradation and
 5 causes a positive ΔV_{FB} as well as a negative ΔN_{ot} .
 6 Furthermore, when radiation passes through a
 7 gate oxide, electron/hole pairs are created
 8 (process (1) in Fig. 5 (a)) [13]. The radiation-
 9 induced electrons escape from the oxide within
 10 several picoseconds due to their higher mobility
 11 relative to holes. Radiation induced holes could
 12 transport towards the AlO_x/Si interface under PBI,
 13 and liberate hydrogen, in the form of protons [14]
 14 which reach the interface by hopping transport
 15 (process (3) in Fig. 5 (a)). The protons can react,
 16 break existing Si-H bonds to form H_2 and a
 17 trivalent Si defect thus causing ΔN_{it} to increase,
 18 as shown in Fig. 4 (b). As mentioned earlier, the
 19 PB is necessary for the de-passivation. Applying
 20 a NB will inhibit the proton from drifting to the
 21 interface and the de-passivation of Si-H bonds by
 22 H at the interface is suppressed [15]. This could
 23 be the reason why ΔN_{it} is found to build up under
 24 PBI, and stay approximately constant under NBI
 25 in Fig. 4 (b).

26 Under NBI, when the stress time is shorter than
 27 2×10^3 s, some of the electrons injected from the
 28 gate electrode into the oxide under the applied
 29 electrical field. They fall into traps to form
 30 negative trapped charges and cause a positive
 31 ΔV_{FB} . Meanwhile, radiation exposure can barely
 32 affect the device degradation. However, as shown
 33 in Fig. 5 (b), in a similar manner to the PBI
 34 condition, accumulated holes at the AlO_x/Si
 35 interface could tunnel from Si to radiation-
 36 induced defects in the oxide to form positive
 37 oxide trapped charges (process (2) in Fig. 5 (b)),
 38 which results in a negative ΔV_{FB} and a positive
 39 ΔN_{ot} as the NBI time increases from 2×10^3 s to
 40 10^5 s.

41 From the analysis above, radiation induces a
 42 large concentration of shallow oxide traps and
 43 causes the generation of interface traps by
 44 releasing protons in solution-processed AlO_x

45 capacitors, thus shifting V_{FB} and degrading the
 46 solution-processed AlO_x MOS capacitors. On the
 47 other hand, ALD AlO_x capacitors show good
 48 radiation hardness and no reversibility of ΔV_{FB} is
 49 observed with biased irradiation. The possible
 50 reason is that the solution-process brings
 51 abundant precursor impurities during fabrication.

52 4. Conclusion

53 Solution-processed and atomic layer deposited
 54 AlO_x thin films were fabricated at low
 55 temperature. The effects of biased irradiation on
 56 AlO_x based MOS capacitors were investigated by
 57 an on-site technique. It has been found that
 58 radiation can result in reversibility of ΔV_{FB} of
 59 solution-processed AlO_x MOS capacitors, which
 60 is further analyzed by extracting the radiation
 61 induced oxide (ΔN_{ot}) and interface (ΔN_{it}) traps at
 62 AlO_x/Si interface. The results suggest that,
 63 compared to the ALD AlO_x films, solution-
 64 processed AlO_x thin films contain abundant
 65 precursor impurities.

66 Acknowledgments

67 This research was funded in part by the Key
 68 Program Special Fund in XJTLU (KSF-P-02,
 69 KSF-A-05, KSF-A-07 and KSF-T-03). The
 70 author IZM acknowledges UKRI GIAA award as
 71 well as British Council UKIERI project no.
 72 IND/CONT/G/17-18/18.

73 References

- 74 [1] W. Xu, M. Long, T. Zhang, L. Liang, H. Cao, D.
 75 Zhu, J.-B. Xu, *Ceramics International* 43 (2017)
 76 6130-6137.
 77 [2] A. Liu, G. Liu, H. Zhu, B. Shin, E. Fortunato, R.
 78 Martins, F. Shan, *RSC Advances* 5 (2015) 86606-
 79 86613.
 80 [3] H.-R. Byun, E.-A. You, Y.-G. Ha, *Appl Phys Lett*
 81 114 (2019) 013301.
 82 [4] R. Lok, S. Kaya, H. Karacali, E. Yilmaz, *Radiat*
 83 *Phys Chem* 141 (2017) 155-159.

1 [5] B. Park, D. Ho, G. Kwon, D. Kim, S. Y. Seo, C.
2 Kim, M.-G. Kim, *Adv Funct Mater* 28 (2018)
3 1802717.
4 [6] Y. Mu, C. Z. Zhao, Q. Lu, C. Zhao, Y. Qi, S.
5 Lam, I. Z. Mitrovic, S. Taylor, P. R. Chalker,
6 *IEEE T Nucl Sci* 64 (2017) 673-682.
7 [7] Y. Mu, C. Z. Zhao, Y. Qi, S. Lam, C. Zhao, Q.
8 Lu, Y. Cai, I. Z. Mitrovic, S. Taylor, P. R.
9 Chalker, *Nucl Instrum Meth B* 372 (2016) 14-28.
10 [8] A. Kahraman and E. Yilmaz, *Radiat Phys Chem*
11 139 (2017) 114-119.
12 [9] J. A. Felix, D. M. Fleetwood, R. D. Schrimpf, J.
13 G. Hong, G. Lucovsky, J. R. Schwank, M. R.
14 Shaneyfelt, *IEEE T Nucl Sci* 49 (2002) 3191-
15 3196.
16 [10] M. Ceschia, A. Paccagnella, A. Cester, A.
17 Scarpa, G. Ghidini, *IEEE T Nucl Sci* 45 (1998)
18 2375-2382.
19 [11] D. A. Neamen, *IEEE T Nucl Sci* 31 (1984)
20 1439-1443.
21 [12] T. Stanley, D. Neamen, P. Dressendorfer, J.
22 Schwank, P. Winokur, M. Ackermann, K.
23 Jungling, C. Hawkins, W. Grannemann, *IEEE T*
24 *Nucl Sci* 32 (1985) 3982-3987.
25 [13] T. R. Oldham and F. B. McLean, *IEEE T Nucl*
26 *Sci* 50 (2003) 483-499.
27 [14] X. J. Zhou, D. M. Fleetwood, L. Tsetseris, R. D.
28 Schrimpf, S. T. Pantelides, *IEEE T Nucl Sci* 53
29 (2006) 3636-3643.
30 [15] D. Cao, X. Cheng, T. Jia, L. Zheng, D. Xu, Z.
31 Wang, C. Xia, Y. Yu, D. Shen, *IEEE T Nucl Sci*
32 60 (2013) 1373-1378.
33
34
35
36
37
38
39